
Research Article: New Research | Sensory and Motor Systems

Choice-Related Activity during Visual Slant Discrimination in Macaque CIP but Not V3A

L. Caitlin Elmore¹, Ari Rosenberg², Gregory C. DeAngelis³ and Dora E. Angelaki¹

¹*Dept. of Neuroscience, Baylor College of Medicine, Houston, TX, 77030, USA*

²*Dept. of Neuroscience, School of Medicine and Public Health, University of Wisconsin - Madison, Madison, WI, 53705, USA*

³*Dept. of Brain and Cognitive Sciences, Center for Visual Science, University of Rochester, NY 14627, USA*

<https://doi.org/10.1523/ENEURO.0248-18.2019>

Received: 22 June 2018

Revised: 18 February 2019

Accepted: 26 February 2019

Published: 7 March 2019

L.C.E. performed research; L.C.E. analyzed data; L.C.E., A.R., G.C.D., and D.E.A. wrote the paper; A.R., G.C.D., and D.E.A. designed research.

Funding: <http://doi.org/10.13039/100000002HHS> | National Institutes of Health (NIH)

R01-EY022538
F32-EY024515
R03-DC014305
R01-EY029438
R01-EY013644

Funding: <http://doi.org/10.13039/100001391Whitehall> Foundation (Whitehall Foundation, Inc.)
2016-08-18

The authors declare no competing financial interests.

L.C.E. and A.R. Equal contribution

Corresponding author: Ari Rosenberg at ari.rosenberg@wisc.edu

Cite as: eNeuro 2019; 10.1523/ENEURO.0248-18.2019

Alerts: Sign up at www.eneuro.org/alerts to receive customized email alerts when the fully formatted version of this article is published.

Accepted manuscripts are peer-reviewed but have not been through the copyediting, formatting, or proofreading process.

Copyright © 2019 Elmore et al.

This is an open-access article distributed under the terms of the Creative Commons Attribution 4.0 International license, which permits unrestricted use, distribution and reproduction in any medium provided that the original work is properly attributed.

1 **Choice-Related Activity during Visual Slant Discrimination in Macaque CIP but Not V3A**

2
3 **Abbreviated Title: Choice Activity during Slant Discrimination**

4
5 L. Caitlin Elmore^{1†}, Ari Rosenberg^{2†*}, Gregory C. DeAngelis³, and Dora E. Angelaki¹

6
7 ¹Dept. of Neuroscience, Baylor College of Medicine, Houston, TX, 77030, USA.

8 ²Dept. of Neuroscience, School of Medicine and Public Health, University of Wisconsin -
9 Madison, Madison, WI, 53705, USA.

10 ³Dept. of Brain and Cognitive Sciences, Center for Visual Science, University of Rochester, NY
11 14627, USA.

12
13 [†]Equal contribution

14 ^{*}Corresponding author

15
16
17 **Author Contributions:** AR, GCD, and DE Designed research; LCE Performed research; LCE
18 Analyzed data; LCE, AR, GCD, and DE Wrote the paper.

19
20
21 **Correspondence:**

22 Ari Rosenberg

23 1111 Highland Ave.

24 WIMR-II, Office 5505

25 Madison, WI. 53705

26 Email: ari.rosenberg@wisc.edu

27
28
29 Number of Figures: 8

30 Number of Tables: 0

31 Number of Multimedia: 0

32 Number of words for Abstract: 183

33 Number of words for Significance Statement: 78

34 Number of words for Introduction: 456

35 Number of words in Discussion: 1533

36
37
38 **Acknowledgments**

39 The authors declare no competing financial interests.

40 This research was supported by NIH grant R01-EY022538 (D.E.A.). L.C.E. was supported by
41 NIH grant F32-EY024515. A.R. was supported by NIH grants R03-DC014305 and R01-
42 EY029438, as well as Whitehall Foundation Research Grant 2016-08-18. G.C.D. was supported
43 by NIH grant R01-EY013644.

44 **Abstract**

45 Creating three-dimensional (3D) representations of the world from two-dimensional retinal
46 images is fundamental to visually guided behaviors including reaching and grasping. A critical
47 component of this process is determining the 3D orientation of objects. Previous studies have
48 shown that neurons in the caudal intraparietal area (CIP) of the macaque monkey represent 3D
49 planar surface orientation (i.e., slant and tilt). Here we compare the responses of neurons in
50 areas V3A (which is implicated in 3D visual processing and which precedes CIP in the visual
51 hierarchy) and CIP to 3D oriented planar surfaces. We then examine whether activity in these
52 areas correlates with perception during a fine slant discrimination task in which monkeys report
53 if the top of a surface is slanted towards or away from them. Although we find that V3A and CIP
54 neurons show similar sensitivity to planar surface orientation, significant choice-related activity
55 during the slant discrimination task is rare in V3A but prominent in CIP. These results implicate
56 both V3A and CIP in the representation of 3D surface orientation, and suggest a functional
57 dissociation between the areas based on slant-related choice signals.

58

59

60

61 **Significance Statement**

62 Surface orientation perception is fundamental to visually guided behaviors such as reaching,
63 grasping, and navigation. Previous studies implicate the caudal intraparietal area (CIP) in the
64 representation of 3D surface orientation. Here we show that responses to 3D oriented planar
65 surfaces are similar in CIP and V3A, which precedes CIP in the cortical hierarchy. However, we
66 also find a qualitative distinction between the two areas: only CIP neurons show robust choice-
67 related activity during a fine visual orientation discrimination task.

68 Introduction

69 Perception of three-dimensional (3D) surface orientation is essential for many visually guided
70 behaviors. Electrophysiological studies have identified 3D orientation selective neurons in
71 multiple brain regions of non-human primates (Murata et al., 2000; Taira et al., 2000; Hinkle and
72 Connor, 2002; Sugihara et al., 2002; Nguyenkim and DeAngelis, 2003; Liu et al., 2004; Durand
73 et al., 2007; Sanada et al., 2012; Alizadeh et al., 2018). In particular, the caudal intraparietal
74 area (CIP) represents all combinations of slant and tilt, two angular variables that specify the 3D
75 orientation of a planar surface (Rosenberg et al., 2013). Anatomical as well as functional
76 magnetic resonance imaging data suggest that V3A, which precedes CIP in the visual
77 hierarchy, may also contribute to 3D visual processing (Nakamura et al., 2001; Tsao et al.,
78 2003). V3A neurons have two-dimensional orientation (Zeki, 1978c, b, a) and binocular disparity
79 (Anzai et al., 2011) tuning, but their responses to 3D surface orientation have not been
80 examined. Moreover, few studies have tested for functional correlations between neuronal
81 activity and 3D orientation perception. Previous work indicates that reversible inactivation of CIP
82 results in small but consistent deficits in a 3D curvature discrimination task (Van Dromme et al.,
83 2016), and may produce a deficit in the ability to perform a delayed match-to-sample task in
84 which planar tilt is coarsely manipulated (Tsutsui et al., 2001).

85 Here we measured the responses of V3A and CIP neurons to 3D surface orientation, as
86 well as their functional correlations with behavior during a fine slant discrimination task. First, 3D
87 surface orientation tuning was measured during a fixation task. The two areas were found to
88 contain similar proportions of selective neurons, as well as similar degrees of selectivity.
89 Second, neuronal activity was recorded while the monkeys viewed planar surfaces at different
90 slants and reported the slant direction in a two-alternative forced-choice task. Receiver
91 operating characteristic (ROC) analysis was used to quantify neuronal sensitivity and to assess
92 choice-related activity (Celebrini and Newsome, 1994; Britten et al., 1996; Dodd et al., 2001;
93 Nienborg and Cumming, 2006; Gu et al., 2007). In contrast to the similarity of stimulus
94 selectivity in the two areas, significant choice-related activity was rare in V3A but prominent in
95 CIP. To further dissociate the contributions of stimulus and choice to neuronal activity, we
96 performed a partial correlation analysis to assess how much variance in the neuronal activity
97 could be attributed to the stimulus and the choice (Zaidel et al., 2017). This analysis confirmed a
98 similar degree of stimulus-related activity in the two areas, and much stronger choice-related
99 activity in CIP than V3A. These results implicate both V3A and CIP in visual surface orientation
100 processing, and demonstrate that binary decision signals during slant discrimination are carried
101 by the most sensitive CIP (but not V3A) neurons.

102 **Materials and Methods**

103 **Subjects and surgery**

104 All surgeries and experimental procedures were approved by the Institutional Animal
105 Care and Use Committees at Washington University in St. Louis and Baylor College of
106 Medicine, and were in accordance with NIH guidelines. Neuronal recordings were obtained from
107 five hemispheres in three male rhesus monkeys (*Macaca mulatta*), denoted as monkeys N, P,
108 and Z, weighing 4-5 kg at the start of the study. As previously described, the monkeys were
109 chronically implanted with a lightweight plastic ring for head restraint, a recording grid, and
110 scleral eye coils for monitoring binocular eye movements (CNC Engineering) (Rosenberg et al.,
111 2013). After recovery, they were trained using standard operant conditioning procedures to
112 fixate visual targets for fluid reward, and to report the direction of surface slant using eye
113 movement responses to targets located above and below the stimulus. After training, neuronal
114 recordings began. We recorded from CIP in two monkeys (N and P), and from V3A in two
115 monkeys (Z and P). Prior to the study, monkey Z underwent a bilateral labyrinthectomy as part
116 of another project. Results from V3A in monkeys Z and P were compared statistically using
117 Wilcoxon rank-sum tests, and no significant differences were found, indicating that the
118 labyrinthectomy had no detectable effects on the current study. Specifically, there were no
119 significant differences in: median choice probability (monkey Z: CP = 0.50; monkey P: CP =
120 0.47; $p = 0.73$), neuronal threshold (monkey Z: 31.29°; monkey P: 23.73°; $p = 0.60$), surface
121 orientation discrimination index (monkey Z: SODI = 0.68; monkey P: SODI = 0.71; $p = 0.89$),
122 squared choice partial correlation (monkey Z: $r^2 = 0.003$; monkey P: $r^2 = 0.01$; $p = 0.20$), and
123 squared slant partial correlation (monkey Z: $r^2 = 0.02$; monkey P: $r^2 = 0.02$; $p = 0.59$). A lack of
124 effects of the labyrinthectomy on visual discrimination is not surprising given that the monkeys
125 were head-fixed during the experiments and that previous studies found that visual heading
126 discrimination performance is largely normal within days following a bilateral labyrinthectomy
127 (Gu et al., 2007).

128

129 **Data acquisition**

130 Epoxy-coated tungsten microelectrodes (Frederick Haer Company, diameter 125 μm ,
131 impedance 1-5 M Ω at 1kHz) were inserted into the cortex through a transdural guide tube using
132 a hydraulic microdrive to record extracellular action potentials. Neuronal voltage signals were
133 amplified, filtered (1Hz – 10 kHz), and displayed on an oscilloscope to isolate single units using
134 a window discriminator (BAK Electronics). Raw voltage signals were digitized at a rate of 25 kHz
135 using a CED Power 1401, and single units were sorted offline as needed (Spike2; Cambridge

136 Electronic Design). In some experiments, action potentials were displayed and isolated using
137 the SortClient software (Plexon).

138 The CARET software was used to segment visual areas in magnetic resonance imaging
139 (MRI) scans of monkeys N and P (Lewis and Van Essen, 2000). Two MRI scans were
140 performed with each of the monkeys. The first (baseline) scan was performed before the head
141 restraint ring was implanted. The second scan was performed after placement of the recording
142 grid in order to align the grid to the baseline MRI images. Recording sites were localized to CIP
143 (which the Lewis and Van Essen Atlas designates as the lateral occipitoparietal zone) using the
144 resulting MRI atlases after alignment of the grids (Van Essen et al., 2001; Rosenberg et al.,
145 2013). When lowering an electrode dorsal-ventrally, CIP was preceded by either the
146 intraparietal sulcus or by cells with prevalent eye-movement responses, depending on the
147 medial-lateral position of the penetration. Once either the intraparietal sulcus or eye-movement
148 responsive cells were passed, neurons were tested for surface orientation selectivity. Neurons
149 in CIP were further identified as having large receptive fields often extending into the ipsilateral
150 visual hemifield (Taira et al., 2000). Area V3A was targeted using the MRI atlas in monkey P
151 and using stereotaxic coordinates in monkey Z. Area V3A is located ventral-lateral and adjacent
152 to CIP. Lateral to CIP and dorsal to V3A is a large patch of white matter. Thus, both CIP and
153 gray/white matter transitions provided landmarks for targeting V3A. As electrodes were
154 advanced dorsal-ventrally, observed gray/white matter transitions were compared with coronal
155 sections to localize V3A. Receptive field mapping was used to compare the receptive field sizes
156 of V3A neurons to previously published data. Receptive field size increased with eccentricity ($r =$
157 0.621 , $p = 0.002$), and the linear fit $y = 0.47x + 1.8$ was similar to previous measurements: $y =$
158 $0.33x + 1.78$ (Galletti and Battaglini, 1989) and $y = 0.38x + 2.8$ (Nakamura and Colby, 2000), as
159 obtained using DataThief (Tummers, 2006). We compared response latency between the areas,
160 and found that V3A neurons (median = 56 ms) responded significantly faster than CIP neurons
161 (median = 72 ms; Wilcoxon rank-sum test, $p = 0.02$).

162

163 **Behavioral control and stimulus presentation**

164 Behavioral control was carried out with custom Spike2 scripts. The monkeys sat in a
165 primate chair ~ 32.5 cm from a liquid crystal display (LCD) on which stimuli were displayed
166 (System 1: NEC Accusync LCD 93VX; System 2: Dell 1707 FP). An aperture constructed from a
167 black non-reflective material was affixed to the screen such that the monkey could only see
168 stimuli within a 30 cm (System 1) or 18 cm (System 2) diameter circular aperture. The same
169 material extended between the LCD and the monkey, occluding the view of the surrounding

170 room. The OpenGL graphics library was used to program visual stimuli that were generated
171 using an OpenGL accelerator board (Quadro FX 3000G, PNY Technologies). The fixation point
172 (yellow in color) was presented directly in front of the monkey at eye level and screen distance.
173 Fixation was enforced using 2° version and 1° vergence windows. Due to eye coil failures in
174 monkey P, the binocular eye movements of this animal were monitored in all experiments using
175 an infrared optical eye tracker (ISCAN).

176

177 **3D surface orientation tuning**

178 Surface orientation tuning was measured as previously described (Rosenberg et al.,
179 2013; Rosenberg and Angelaki, 2014a, b). Briefly, a planar surface with a checkerboard pattern
180 was used to measure the joint tuning for slant and tilt (Fig. 1A). Stimuli subtended either 50° or
181 31° of visual angle. Initial recordings with monkey N were conducted in System 1 (used in our
182 previous CIP studies) which allowed us to present 50° stimuli (30 neurons). However, monkey N
183 outgrew the system, which only accommodates relatively small animals. The remaining data for
184 monkey N (14 neurons) and all data from monkeys P and Z were gathered in System 2, for
185 which the largest possible stimulus was 31°. Wilcoxon rank-sum tests revealed no significant
186 differences in the results for monkey N across the two systems, including comparisons of
187 median values of: choice probability (System 1: CP = 0.57; System 2: CP = 0.58; $p = 0.44$),
188 neuronal threshold (System 1: 37.96°; System 2: 31.79°; $p = 0.89$), behavioral threshold
189 (System 1: 3.60°; System 2: 3.74°; $p = 0.27$), point of subjective equality (System 1: 0.16°;
190 System 2: -0.71°; $p = 0.13$), squared choice partial correlation (System 1: $r^2 = 0.02$; System 2: r^2
191 = 0.009; $p = 0.47$), and squared slant partial correlation (System 1: $r^2 = 0.01$; System 2: $r^2 =$
192 0.02; $p = 0.97$).

193 Slant was varied between 0° and 60° in 20° steps, and tilt was varied between 0° and
194 315° in 45° steps. All stimuli were centered on the fixation point and covered the same
195 retinotopic area. Stereoscopic cues were created by rendering the stimuli as red-green
196 anaglyphs. Each trial began with the monkey fixating a point on a blank screen for 300 ms.
197 Fixation was maintained while a checkerboard stimulus was presented for 1,000 ms, followed
198 by 50 ms of fixation with a blank screen. There was a 1,000 ms blank screen inter-trial interval.
199 Stimuli were presented in pseudo-random order. Surface orientation selectivity was assessed
200 for all cells held for at least three repetitions of each stimulus. At most seven repetitions of each
201 stimulus were recorded. For each selective neuron (see Results), a one-way ANOVA was
202 performed to determine if there was significant slant tuning along the 90°/270° tilt axis (see Figs.
203 1A, 3A,B). Neurons with significant tuning were studied further in the slant discrimination task.

204

205 Slant discrimination task

206 The slant discrimination task was always performed along the $90^{\circ}/270^{\circ}$ tilt axis. To
207 simplify the description of surface orientation, we do not refer to tilt for the slant discrimination
208 task but instead denote planes with a tilt of 90° (top of the plane closer to the monkey) as having
209 a negative slant, and planes with a tilt of 270° (top of the plane further from the monkey) as
210 having a positive slant (c.f., Rosenberg and Angelaki, 2014b). As illustrated in Fig. 2A, each trial
211 of the slant discrimination task began with the monkey fixating a target on a blank screen for
212 300 ms after which a random dot stereogram (RDS) depicting a planar surface was presented
213 for 1,000 ms. After presentation of the RDS, the fixation point disappeared, and two choice
214 targets appeared 8.6° above/below the location of the fixation point. The monkey then made an
215 eye movement to one of the choice targets to indicate the perceived slant. Correct responses
216 were defined as a saccade to the upper target when the slant was positive (top-far) or to the
217 lower target when the slant was negative (top-near). Correct responses were rewarded with a
218 drop of water or juice. For planes with slant = 0° (i.e., frontoparallel), responses were rewarded
219 pseudo-randomly 50% of the time. If the monkey broke fixation at any point during the stimulus
220 presentation, the trial was aborted and the data discarded.

221 During pilot work, we observed that local orientation cues in checkerboard stimuli could
222 be used to perform the task without having to judge slant. To avoid this potential confound, the
223 discrimination task was performed using RDS planes with uniform dot density on the screen
224 (Sanada et al., 2012). In CIP, slant tuning curves measured with planar surfaces with a
225 checkerboard pattern or a random dot pattern are highly correlated (Rosenberg and Angelaki,
226 2014b). To discourage the monkeys from using local depth cues to perform the task (Hillis et al.,
227 2004), we varied the mean depth (near = -2.25 cm from the screen, screen distance = 0 cm, far
228 = 2.25 cm from the screen) of the RDS plane from trial to trial (Fig. 2B). This discouraged them
229 from judging whether the upper (lower) half of the stimulus was in front of (behind) the plane of
230 the display. If the animals relied on the absolute disparity of a sub-region of the stimulus to
231 perform the task, large behavioral biases would result at the near/far depths. For the 31°
232 stimulus, biases of at least 14° in magnitude (the slant at which a stimulus would start to cross
233 the screen) would occur in opposite directions for the near and far depths. Behavioral data
234 clearly show this was not the case (Fig. 2C,D), suggesting that the animals correctly learned to
235 judge the sign of slant. To maintain this behavior during the neuronal recordings, stimuli were
236 presented at screen distance for 70% of trials, the near depth for 15% of trials, and the far depth

237 for 15%. For the neuronal recordings, there was sufficient data to reliably analyze the responses
238 measured at screen distance only.

239 Slant was varied between $\pm 20^\circ$ with the intermediate slants tailored to each monkey's
240 performance. For monkeys N and Z, slants of $\pm 20^\circ$, 10° , 5° , 2.5° , 1.25° , and 0° were used. For
241 monkey P, slants of $\pm 20^\circ$, 9° , 4.05° , 1.83° , 0.82° , and 0° were used. Neurons were recorded
242 while the monkey performed the task for a minimum of 10 repetitions of each stimulus. Sufficient
243 repetitions were recorded for 65 CIP and 23 V3A neurons.

244

245 **Data analysis**

246 Analyses were performed in MATLAB (*MathWorks*). Unless otherwise noted, analyses
247 were performed on firing rates or spike counts computed during the 1,000 ms stimulus
248 presentation period. The tuning strength of each neuron was evaluated using a surface
249 orientation discrimination index (SODI), motivated by previous studies (Prince et al., 2002), that
250 was calculated using the full slant-tilt tuning curve. The SODI quantifies the strength of
251 response modulation relative to overall response variability:

$$252 \quad SODI = \frac{R_{max} - R_{min}}{R_{max} - R_{min} + 2\sqrt{SSE/(N-M)}} \quad (\text{Eq. 1})$$

253 where R_{max} and R_{min} are the maximum and minimum responses, respectively. SSE denotes the
254 sum squared error around the mean responses, N is the total number of trials, and M is the
255 number of tested slant-tilt combinations ($M = 25$). Neurons with strong response modulation
256 relative to their variability have SODI values closer to 1, whereas neurons with weak response
257 modulation have SODI values closer to 0.

258 Behavioral performance in the slant discrimination task was quantified by plotting the
259 proportion of top-far choices as a function of stimulus slant. The resulting psychometric function
260 was fit with a cumulative Gaussian using the Psignifit toolbox (Wichmann and Hill, 2001). The
261 point of subjective equality and behavioral threshold were defined as the mean and standard
262 deviation of the cumulative Gaussian fit, respectively.

263 Neuronal sensitivity was measured by using ROC analysis to assess the ability of an
264 ideal observer to discriminate between two opposite slants (e.g., -20° from $+20^\circ$; Fig. 3E,F)
265 based on the firing rate of a recorded neuron and a hypothetical 'anti-neuron' with opposite
266 tuning (Britten et al., 1996; Gu et al., 2007). To construct a neurometric function that could be
267 directly compared to the psychometric function (Fig. 4A,B), ROC values were plotted as a
268 function of slant and fit with a cumulative Gaussian using the Psignifit toolbox. Neuronal
269 threshold (an inverse measure of sensitivity) was defined as the standard deviation of the
270 cumulative Gaussian fit. Neuronal and behavioral thresholds were calculated from

271 simultaneously gathered data, allowing for a direct comparison. For this comparison, neuronal
272 thresholds were multiplied by $\sqrt{2}$ to account for the behavioral task being conducted as a one
273 interval task (Hillis et al., 2004), but the neurometric functions being calculated by comparing
274 two distributions (the neuron and its hypothetical anti-neuron). The time course of neuronal
275 sensitivity was assessed by computing neuronal thresholds in 200 ms time windows, starting at
276 100 ms after stimulus onset, and shifted every 50 ms over the 1,000 ms stimulus duration.

277 To quantify the relationship between neuronal response and choice, choice probabilities
278 (CPs) were computed using ROC analysis. For each slant, neuronal responses were grouped
279 according to the choice. 'Preferred' choices corresponded to those made in favor of the
280 neuron's preferred slant, as determined from the 3D surface orientation tuning profile measured
281 during fixation. 'Non-preferred' choices corresponded to those made in the opposite direction.
282 CP was computed by performing ROC analysis on the preferred and non-preferred choice
283 distributions for the (ambiguous) 0° slant stimulus. To achieve greater statistical power, a grand
284 CP was computed by performing ROC analysis after normalizing the neuronal responses for
285 each stimulus slant and combining the normalized data into two composite distributions
286 corresponding to preferred versus non-preferred choices (Kang and Maunsell, 2012). Only
287 stimulus slants for which the monkey made at least 3 choices in each direction were included in
288 the grand CP calculation. To test if CPs were significantly different from chance level (CP =
289 0.50), a permutation test was used (1,000 permutations). The time course of choice-related
290 activity was measured by computing CPs in 200 ms time windows, starting at 100 ms after
291 stimulus onset, and shifted every 50 ms. The last time window was centered 150 ms after the
292 stimulus offset (1,150 ms after stimulus onset). In this way, the time course of choice-related
293 activity included responses up to approximately the median choice time (271 ms after stimulus
294 offset).

295 To quantify the contributions of stimulus slant and choice to the responses of each
296 neuron, Pearson correlations were computed between the following variables: slant, choice, and
297 neuronal spike count. From these correlations, we computed a slant partial correlation, $r_{FS,C}$ (Eq.
298 2), that quantifies the relationship between spike count (F) and slant (S) while controlling for
299 choice (C), and a choice partial correlation, $r_{FC,S}$ (Eq. 3), that quantifies the relationship between
300 spike count and choice while controlling for slant. Because this analysis assumes a linear
301 relationship between the stimulus and firing rate over the range of tested slants, we confirmed
302 that the pattern of results did not change if slant was replaced with a nonlinear slant function
303 including cubic, exponential, and sigmoidal functions, or if a larger partial correlation analysis
304 was run which included multiple slant functions including the linear term. We did not consider

305 nonlinear functions of choice because choice was a binary variable. Because the pattern of
 306 results did not depend appreciably on the stimulus function, as also reported recently for
 307 heading discrimination in the ventral intraparietal area (Zaidel et al., 2017), only the partial
 308 correlation analysis performed with slant, choice, and spike count is presented.

$$309 \quad r_{FS,C} = \frac{r_{FS} - r_{FC}r_{SC}}{\sqrt{(1-r_{FC}^2)(1-r_{SC}^2)}} \quad (\text{Eq. 2})$$

$$310 \quad r_{FC,S} = \frac{r_{FC} - r_{FS}r_{SC}}{\sqrt{(1-r_{FS}^2)(1-r_{SC}^2)}} \quad (\text{Eq. 3})$$

311 Positive slant partial correlations indicate that spike counts were greater for positive
 312 slants than negative slants. Positive choice partial correlations indicate that spike counts were
 313 greater for top-far than top-near choices. Partial correlations were computed based on spike
 314 counts over the entire 1,000 ms stimulus duration. For the time course analyses, partial
 315 correlations were computed in 200 ms time windows, starting at 100 ms after stimulus onset,
 316 and shifted every 50 ms. The last bin center was 1,150 ms after stimulus onset. For the partial
 317 correlation time course analysis, partial correlations were squared to determine how much
 318 variance in the spike counts was accounted for by stimulus and choice.

319

320 Results

321 Comparison of CIP and V3A responses to 3D surface orientation

322 Surface orientation tuning was measured for 427 CIP and 72 V3A neurons during a
 323 fixation task in which a checkerboard plane was presented at 25 slant-tilt combinations (Fig.
 324 1A). Of these, 396 CIP (93%) and 60 V3A (83%) neurons were held for enough repetitions (≥ 3)
 325 to assess tuning. Tuning strength was quantified using a surface orientation discrimination index
 326 (SODI; see Materials and Methods) which ranges from 0 to 1. Larger SODI values indicate
 327 stronger tuning. The mean SODI in CIP was 0.63 ± 0.005 SEM (N = 396; Fig. 1B), and in V3A it
 328 was 0.68 ± 0.02 SEM (N = 60; Fig. 1C). The mean SODI was significantly smaller in CIP than
 329 V3A (Wilcoxon rank sum test, $p = 5.8 \times 10^{-4}$).

330 A two-step procedure was used to classify neurons as tuned or untuned. First, a one-
 331 way ANOVA was performed on the firing rates in response to each of the 25 slant-tilt
 332 combinations. Second, the tuning curve of each neuron that passed the ANOVA ($p < 0.05$) was
 333 fit with a Bingham function (Rosenberg et al., 2013). The second step eliminates neurons with
 334 multiple tuning peaks which would pass an ANOVA but are not selective for a unique stimulus
 335 (see Figure 5 in Rosenberg et al., 2013). Neurons with a Pearson correlation for the Bingham fit
 336 ≥ 0.8 were classified as tuned, and otherwise untuned. Based on these criteria, 215 CIP

337 neurons (54% of the 396 tested) and 44 V3A neurons (73% of the 60 tested) were tuned. Of the
338 neurons classified as untuned, 26.5% in CIP (48/181) and 25% in V3A (4/16) were rejected for
339 having multiple peaks.

340 The distribution of slant–tilt preferences was examined for each area by performing an
341 equal area preserving projection (Rosenberg et al., 2013) and plotting the preferred slant and tilt
342 of each neuron in that space (Fig. 1D). We previously found that the distribution of CIP slant–tilt
343 preferences was not significantly different from uniform in untrained animals (Rosenberg et al.,
344 2013). Here we found that the distribution of preferences in CIP and V3A were significantly
345 different from uniform (Chi-squared test, CIP: $p = 1.07 \times 10^{-7}$; V3A: $p = 0.01$). In particular, there
346 was a bias towards representing smaller slants (note the relative sparsity of cells near the top of
347 the scatter plot in Fig. 1D). It is possible that extensive training in the fine slant discrimination
348 task resulted in a shift in tuning preferences towards smaller slants.

349

350 **Slant discrimination behavior**

351 A control experiment was conducted to confirm that the animals did not perform the slant
352 discrimination task based on local absolute disparity cues signaling that the upper (lower) half of
353 the plane was in front of (behind) the LCD. Each monkey performed the slant discrimination task
354 for nine sessions with the stimuli centered at three depths (0 and ± 2.25 cm) from the display
355 (Fig. 2A,B). Psychometric functions for each monkey and depth are shown in Fig. 2C. The
356 proportion of ‘top-far’ choices is plotted for each slant and fit with a cumulative Gaussian
357 function. One-way ANOVAs showed no significant effect of depth on the point of subjective
358 equality (P.S.E.; monkey N: $F = 0.65$, $p = 0.53$; monkey P: $F = 0.53$, $p = 0.60$; monkey Z: $F =$
359 2.41 , $p = 0.12$) or threshold (monkey N: $F = 0.58$, $p = 0.57$; monkey P: $F = 0.11$, $p = 0.90$;
360 monkey Z: $F = 0.70$, $p = 0.51$). Although not significant, there was a slight tendency for the
361 P.S.E. to be negative at -2.25 cm (Fig. 2D). However, if the animals were relying on local
362 absolute disparity cues to perform the task, the P.S.E. would have a magnitude of at least 14° at
363 the near/far depths (i.e., the smallest slant at which a plane would cross the screen), which is
364 much greater than the average P.S.E. of -0.38° at -2.25 cm. One-way ANOVAs also revealed
365 that there was no significant effect of stimulus depth on mean vergence angle during the
366 stimulus presentation (monkey N: $F = 0.42$, $p = 0.70$; monkey P: $F = 3.57 \times 10^{-4}$, $p = 0.99$; monkey
367 Z: $F = 0.50$, $p = 0.66$), suggesting that the slightly negative P.S.E. at -2.25 cm was not due to a
368 systematic vergence error. These data strongly suggest that the monkeys performed the task by
369 assessing the slant of the plane rather than by judging local stimulus depth relative to the plane
370 of fixation.

371

372 **Neuronal sensitivity during slant discrimination**

373 Of the 215 tuned CIP neurons, 151 (70%) were significantly tuned for slant (ANOVA, $p <$
374 0.05) along the $90^\circ/270^\circ$ tilt axis used in the slant discrimination task (white dashed lines in Fig.
375 3A,B), and therefore studied further. Of these, data from 65 (43%) were included in this study.
376 The remaining 86 neurons (57%) were recorded for another task (16 neurons, 11%) or were not
377 recorded for a sufficient number of repetitions (≥ 10) to be included (70 neurons, 46%).
378 Likewise, of the 44 V3A neurons, 35 (80%) were significantly tuned for slant along the $90^\circ/270^\circ$
379 tilt axis. Of these, 23 (66%) were held for sufficient repetitions (≥ 10) to be included.

380 Surface orientation tuning curves for example CIP and V3A neurons that met these
381 criteria are shown in Fig. 3A,B. Responses recorded during the slant discrimination task are
382 shown in Fig. 3C,D for the same neurons. For both neurons, tuning was monotonic over the
383 range of slants presented in the discrimination task. The CIP neuron (Fig. 3C) fired more in
384 response to positive slants (top of the plane further from the animal), whereas the V3A neuron
385 (Fig. 3D) fired more in response to negative slants (top of the plane closer to the animal).

386 To assess how well the responses of these neurons could be used to discriminate slants
387 of opposite sign, we compared firing rate distributions. Firing rate distributions for 3 pairs of
388 slants ($\pm 20^\circ$, $\pm 5^\circ$, and $\pm 1.25^\circ$) are shown in Fig. 3E,F. Note that the distributions are completely
389 overlapping for $\pm 1.25^\circ$ whereas there is little or no overlap at $\pm 20^\circ$. Consequently, an ideal
390 observer could reliably discriminate $\pm 20^\circ$ of slant based on the firing rates of these neurons, but
391 would be unable to discriminate $\pm 1.25^\circ$ of slant. The ability of an ideal observer to discriminate
392 slants of opposite sign was quantified using ROC analysis (Britten et al., 1996; Gu et al., 2007).
393 The probability that an ideal observer could correctly report whether the slant of a presented
394 plane was positive or negative was calculated for each slant magnitude. A neurometric function
395 was then constructed by plotting ROC values for each slant pair (i.e., positive and negative
396 slants of the same magnitude), and fitting the function with a cumulative Gaussian (Fig. 4A,B,
397 solid curves). A neuronal threshold quantifying the neuron's sensitivity to changes in slant was
398 defined as the standard deviation of the cumulative Gaussian fit. This analysis was performed
399 for each of the 65 CIP and 23 V3A neurons, and the resulting neurometric functions are shown
400 in Fig. 4C,D. Across all monkeys, the median neuronal thresholds were 32.86° in CIP and
401 26.25° in V3A, and were not significantly different (Wilcoxon rank sum test, $p = 0.48$). We further
402 confirmed that neuronal thresholds were similar between monkeys. The median CIP thresholds
403 were 35.16° (monkey N) and 26.04° (monkey P), and not significantly different (Wilcoxon rank
404 sum test, $p = 0.30$). Likewise, the median V3A thresholds were 31.30° (monkey Z) and 23.73°

405 (monkey P), and not significantly different (Wilcoxon rank sum test, $p = 0.58$). These results
406 indicate that CIP and V3A neurons are similarly sensitive to changes in slant.

407 Neurometric functions can be directly compared to psychometric functions measured in
408 the same recording session (dashed curves, Fig. 4A,B). Simultaneously measured neuronal and
409 behavioral thresholds are compared in Fig. 4E,F for CIP and V3A, respectively. For this
410 comparison, neurometric thresholds were multiplied by $\sqrt{2}$ since the neurometric functions were
411 constructed by comparing two response distributions (the neuron/anti-neuron approach),
412 whereas the behavioral task had a single stimulus interval. Distributions of neuronal to
413 behavioral threshold ratios are shown as diagonal histograms. All of the neuronal/behavioral
414 threshold ratios were greater than 1, indicating that no recorded CIP or V3A neuron was more
415 sensitive than the monkey. Monkey N's median neuronal/behavioral threshold ratio was 14 for
416 CIP, monkey P's median threshold ratio was 34 for CIP and 30 for V3A, and monkey Z's median
417 threshold ratio was 16 for V3A. Although behavioral sensitivity was greater than neuronal
418 sensitivity, the thresholds of some neurons approached that of the behavior, suggesting that
419 CIP and V3A could contribute to performance of the slant discrimination task.

420

421 **Neuronal responses in CIP but not V3A correlated with slant reports**

422 During the slant discrimination task, variability was observed in both the neuronal firing
423 rates and choices elicited by stimuli of the same slant. This variability is evident in histograms of
424 the example CIP neuron's responses to a slant of 0° , grouped by choice (Fig. 5A). This stimulus
425 is ambiguous and there is no correct answer because the top of the plane leans neither toward
426 nor away from the monkey. Thus, the monkey made choices toward both response targets with
427 roughly equal frequency. For the example CIP neuron, the firing rate tended to be lower when
428 the monkey made a top-near choice and greater when the monkey made a top-far choice. In
429 other words, responses were greater when the monkey chose the target corresponding to the
430 neuron's slant preference. In contrast, the example V3A neuron preferred negative slants, but
431 the histograms of responses to a slant of 0° , grouped by choice, were largely overlapping. Thus,
432 there was no clear difference in the activity of the example V3A neuron when the animal made
433 top-far versus top-near choices (Fig. 5B).

434 Choice probability (CP) analysis was used to quantify the relationship between neuronal
435 response and choice (Celebrini and Newsome, 1994; Britten et al., 1996; Dodd et al., 2001;
436 Nienborg and Cumming, 2006; Gu et al., 2007). We computed the CP by first assigning
437 neuronal responses, calculated over the 1,000 ms stimulus presentation period, to two groups
438 according to the monkey's choice. 'Preferred' slant choices were made in the direction of the

439 preferred slant and 'non-preferred' slant choices were made in the direction of the non-preferred
440 slant. Preferred and non-preferred slants were defined according to the tuning preference along
441 the 90°/270° tilt axis that was measured during the 3D orientation tuning (fixation only) task.
442 Slant preferences generally matched between the fixation and discrimination tasks, with the
443 preference reversing for only 6 CIP neurons and 1 V3A neuron. Since reversals of slant
444 preference could be an effect of choice-related signals during the discrimination task, we
445 computed CPs based on stimulus preferences measured during fixation.

446 After sorting responses by choice, we used ROC analysis to compute the probability
447 that an ideal observer could predict the monkey's choice based on the neuron's responses (see
448 Materials and Methods). The CP was calculated in two ways. First, we only considered
449 responses to the ambiguous 0° slant stimulus. For the CIP neuron in Fig. 5A, the CP was 0.65,
450 indicating it fired more when the monkey made a choice in favor of the preferred slant. Across
451 all CIP neurons, the mean CP for a 0° slant stimulus was 0.58, which was significantly greater
452 than the chance value of 0.50 (t -test, $t = 3.89$, $p = 2.45 \times 10^{-4}$). For the V3A neuron in Fig. 5B, the
453 CP was 0.45, suggesting the neuron fired slightly more when the monkey made a choice in
454 favor of the cell's non-preferred slant. Across all V3A neurons, the mean CP for the 0° slant
455 stimulus was 0.52, which was not significantly different from chance (t -test, $t = 0.64$, $p = 0.53$).
456 Second, to achieve greater statistical power, we calculated a 'grand CP' by including responses
457 to all slants for which the monkey made at least 3 choices toward each response target. For this
458 analysis, responses to each slant were normalized using the balanced Z-score method (Kang
459 and Maunsell, 2012). For the CIP neuron in Fig. 5A, the grand CP was 0.65 and significantly
460 greater than the chance value of 0.50 (permutation test, 1000 permutations, $p = 0.001$). The
461 grand CP for the V3A neuron in Fig. 5B was 0.50 and not significantly different from chance ($p =$
462 0.36). Across the neural populations, the grand CP was highly correlated with the CP measured
463 for the 0° slant stimulus (CIP: $r = 0.81$, $p = 1.0 \times 10^{-15}$; V3A: $r = 0.78$, $p = 0.0001$). The analyses
464 that follow are based on grand CPs.

465 Histograms of CP for CIP and V3A are shown in Fig. 5C,D. The mean CIP CP was 0.57,
466 which was significantly greater than 0.50 (t -test, $p = 1 \times 10^{-15}$). The mean CIP CP was also
467 significantly different from chance for each monkey (t -test, monkey N: CP = 0.57, $p = 3.40 \times 10^{-4}$;
468 monkey P: CP = 0.57, $p = 0.04$). In total, 51% of CIP neurons (33/65) had CPs that were
469 significantly different from chance (permutation test, 1000 permutations, $p < 0.05$). For the
470 majority of CIP neurons with significant CPs (26/33), firing rates increased when the monkey
471 made a choice in favor of the preferred slant (CPs > 0.50). However, 7 CIP CPs were
472 significantly below 0.50, indicating they fired more when the monkey made a choice in favor of

473 the non-preferred slant. In contrast to CIP, the mean V3A CP was 0.48, which was not
474 significantly different from 0.50 (t -test, $p = 0.40$). Neither monkey had a mean V3A CP that was
475 significantly different from chance (t -test, monkey P: CP = 0.48, $p = 0.42$; monkey Z: CP = 0.49,
476 $p = 0.67$). Permutation tests revealed that only one V3A neuron had a CP that was significantly
477 different from chance. As a control, we confirmed that there was no significant difference in CP
478 associated with whether the neurons preferred positive or negative slants. The mean CIP CP
479 was 0.55 ± 0.03 SEM ($N = 30$) for neurons preferring positive slants and 0.59 ± 0.03 SEM ($N =$
480 35) for those preferring negative slants (t -test, $t = 1.49$, $p = 0.14$). The mean V3A CP was $0.46 \pm$
481 0.03 SEM ($N = 10$) for neurons preferring positive slants and 0.50 ± 0.03 SEM ($N = 13$) for those
482 preferring negative slants (t -test, $t = 1.29$, $p = 0.21$). Comparing choice-related activity across
483 the two areas, we found that the mean CIP CP was significantly greater than the mean V3A CP
484 (t -test, $p = 0.003$). These findings indicate that the CIP, but not V3A, neurons displayed strong
485 choice related activity during the slant discrimination task.

486 We further found that the CIP neurons showed a significant negative correlation between
487 neuronal threshold and CP ($r = -0.44$, $p = 3 \times 10^{-4}$; Fig. 5E). The 10 most sensitive CIP neurons
488 had a mean CP of 0.72 ± 0.03 (SEM), whereas the 10 least sensitive had a mean CP of $0.48 \pm$
489 0.03 (SEM). In contrast, the correlation between neuronal threshold and CP was not significant
490 in V3A ($r = -0.20$, $p = 0.36$), and the V3A CPs clustered around 0.50 regardless of neuronal
491 threshold (Fig. 5F). We additionally ran an ANCOVA in which CP was the dependent variable,
492 neuronal threshold was a continuous covariate, and brain area was an ordinal factor. We found
493 a significant interaction ($p = 0.03$) between neuronal threshold and brain area, indicating a
494 significant difference in the strength of the relationship between CP and neuronal threshold in
495 CIP and V3A.

496 As a control, we confirmed that trial-by-trial variation in vertical eye position, vertical eye
497 velocity, and vergence during the stimulus presentation had no appreciable effect on CIP CPs
498 and neuronal thresholds (Gu et al., 2007). For each CIP neuron, we performed three separate
499 analyses of covariance (ANCOVAs) to test the relationship between neuronal firing rate and
500 choice with vertical eye position, vertical eye velocity, or vergence as co-regressors (averaged
501 over the length of each trial). Fifteen percent (10/65) of CIP neurons had a significant
502 dependence of firing rate on vertical eye position, 3% (2/65) had a significant dependence of
503 firing rate on vertical eye velocity, and 6% (4/65) had a significant dependence of firing rate on
504 vergence ($p < 0.05$, ANCOVA, Bonferroni-Holm correction for multiple comparisons). We
505 therefore calculated CPs and neuronal thresholds after removing the dependence (linear trend)
506 on vertical eye position, vertical eye velocity, and vergence from the neuronal responses. After

507 removing the effect of vertical eye position, there was a small but significant reduction in CP
508 (0.57 before versus 0.56 after correction; paired t -test, $t = 2.53$, $p = 0.01$). The CP
509 measurements before and after correction were highly correlated ($r = 0.96$, $p = 1.0 \times 10^{-16}$), and
510 the mean value remained significantly greater than chance after correction (t -test, $t = 3.61$, $p =$
511 5.95×10^{-4}). Removal of the effect of vertical eye position had no significant effect on the median
512 neuronal threshold (Wilcoxon sign-rank test, $p = 0.24$). For vertical eye velocity, there was a
513 small but significant effect on the mean CP (0.57 before versus 0.56 after correction, paired t -
514 test, $t = 3.05$, $p = 0.003$) and the median neuronal threshold (32.86° before versus 38.06° after
515 correction, Wilcoxon sign-rank test, $p = 0.03$). The CP measurements before and after
516 correction were highly correlated ($r = 0.95$, $p = 1.0 \times 10^{-16}$), and remained significantly greater
517 than chance after correction (t -test, $t = 3.57$, $p = 6.92 \times 10^{-4}$). Neuronal thresholds were also
518 highly correlated before and after correction ($r = 0.85$, $p = 3.0 \times 10^{-15}$). For vergence, there was
519 no significant effect on mean CP ($p = 0.58$) or median neuronal threshold ($p = 0.48$). Thus,
520 variations in eye position, eye velocity, and vergence had little effect on CIP CPs and neuronal
521 thresholds.

522

523 **Contributions of stimulus and choice to CIP and V3A responses**

524 During the slant discrimination task, both the stimulus and the choice may contribute to
525 neuronal activity. The contributions of stimulus and choice to the activity of example CIP and
526 V3A neurons is shown in Fig. 6. Slant tuning curves measured by averaging firing rates across
527 all presentations of each slant, without regard to the choice, are shown in black. For
528 comparison, choice-conditioned slant tuning curves were computed for top-far and top-near
529 choices (orange and purple curves in Fig. 6, respectively). Only slants for which the monkey
530 made at least three choices in the relevant direction were included in the choice-conditioned
531 tuning curves. In CIP, choice-conditioned tuning curves often showed clear separation,
532 indicating a strong effect of choice on firing rate. For the CIP neuron in Fig. 6A, the top-far
533 choice-conditioned tuning curve (orange) lies above the top-near choice-conditioned tuning
534 curve (purple). This difference indicates the neuron responded more strongly when the monkey
535 made a choice in the direction of the neuron's preferred slant (top-far). Correspondingly, the
536 neuron's CP is greater than 0.50. In contrast, Fig. 6B shows a CIP neuron that responded more
537 strongly when the monkey made a choice in the opposite direction of the preferred slant. Hence,
538 the top-near choice-conditioned tuning curve (purple) is above the top-far choice-conditioned
539 tuning curve (orange), and the CP is less than 0.50. In V3A, choice-conditioned tuning curves

540 largely overlapped. This was the case even when the CP was relatively large, as shown for the
541 neuron in Fig. 6C, indicating that choice had little effect on V3A responses.

542 To dissociate the contributions of stimulus and choice to each neuron's responses,
543 partial correlations were computed between slant, choice, and spike counts (over the 1,000 ms
544 stimulus presentation period) using all trials. This analysis estimates how much variance in the
545 responses can be accounted for by stimulus and choice while controlling for the fact that these
546 variables are correlated. Similar percentages of CIP (30/65; 46%) and V3A (10/23; 43%)
547 neurons had significant slant partial correlations ($p < 0.05$), and the magnitude (absolute value)
548 of the slant partial correlations in CIP (median = 0.09) and V3A (median = 0.15) were not
549 significantly different (Wilcoxon rank-sum test, $p = 0.14$). The ranges of slant partial correlations
550 in CIP ($r = -0.51$ to 0.47) and V3A ($r = -0.48$ to 0.46) were also similar. Correspondingly, the
551 variance of the slant partial correlations was not significantly different between the areas
552 (Levene's test, $W = 2.11$, $p = 0.15$).

553 Although the slant partial correlations in CIP and V3A were similar, the choice partial
554 correlations differed substantially. A greater percentage of neurons had significant choice partial
555 correlations in CIP (40/65; 62%) than V3A (7/23; 30%), and the magnitude of the choice partial
556 correlations in CIP (median = 0.13) was significantly greater than in V3A (median = 0.09),
557 Wilcoxon rank-sum test ($p = 0.003$). The range of choice partial correlations was also greater in
558 CIP ($r = -0.55$ to 0.49) than V3A ($r = -0.15$ to 0.20). Correspondingly, the variance of the choice
559 partial correlations was significantly different between the areas (Levene's test, $W = 9.19$, $p =$
560 0.003). These findings confirm that choice had a greater effect on CIP than V3A activity.

561 In CIP, the relative signs of the slant and choice partial correlations were largely
562 predictive of CP. The CIP neuron in Fig. 6A preferred positive slants (positive slant partial
563 correlation) and top-far choices (positive choice partial correlation). Consistent with this, the CP
564 was significantly greater than 0.50 ($p = 0.001$). In contrast, the CIP neuron in Fig. 6B preferred
565 positive slants (positive slant partial correlation) but top-near choices (negative choice partial
566 correlation). Consistent with this, the CP was significantly less than 0.50 ($p = 0.001$). For
567 comparison, a V3A neuron that preferred negative slants and top-near choices is shown in Fig.
568 6C. Although the CP was greater than 0.50, it was not significantly different from 0.50 ($p =$
569 0.29).

570 The relationships between slant partial correlation, choice partial correlation, and CP are
571 summarized for CIP and V3A in Fig. 7. Quadrant I (upper right) contains neurons for which
572 positive slants and top-far choices increased firing rate. Quadrant III (lower left) contains
573 neurons for which negative slants and top-near choices increased firing rate. Note that top-far

574 (top-near) choices were correct for positive (negative) slants; thus, quadrants I and III contain
575 neurons with congruent stimulus and choice effects. Based on the example cells in Fig. 6,
576 quadrants I and III should contain neurons with CPs greater than 0.50, at least in CIP where
577 choice effects are robust. Consistent with this prediction, the CP of 35/40 (88%) of the CIP
578 neurons in quadrants I and III was greater than 0.50 (Fig. 7A) and the mean CP was 0.59 ± 0.02
579 (SEM, $N = 40$), which was significantly greater than 0.50 (Wilcoxon signed rank test, $p = 3.3 \times 10^{-6}$).
580

581 There was also a substantial number of neurons for which slant and choice had opposite
582 effects on firing rate (quadrants II and IV). Cells in quadrant II (upper left) are those for which
583 firing rate increased for negative slants and top-far choices. Cells in quadrant IV (lower right) are
584 those for which firing rate increased for positive slants and top-near choices. Assuming that CP
585 was computed based on the true sign of the slant preference (determined from the surface
586 orientation tuning curve measured during fixation to minimize choice-related activity; the sign
587 reversed for one CIP neuron in quadrants II/IV if determined from the slant discrimination data),
588 neurons in quadrants II and IV should have CPs less than 0.50. This was not immediately
589 evident: 12/25 (48%) CIP neurons in these quadrants had CPs less than 0.50, and the mean CP
590 = 0.50 ± 0.02 SEM was not significantly different from 0.50 ($N = 25$, Wilcoxon signed rank test, p
591 = 0.95). Note, however, that neurons with the lowest CPs (darker blue points) are largely found
592 in quadrants II and IV.

593 To further test if CPs are related to the relative signs of the slant and choice partial
594 correlations, we fit a 95% confidence ellipse to the data from all CIP neurons with CPs > 0.50
595 (green dashed ellipse) and a 95% confidence ellipse to those with CPs < 0.50 (blue solid
596 ellipse), as shown in Fig. 7A. Consistent with our predictions, the ellipses are obliquely oriented
597 and nearly orthogonal. The orientation of the major axis for the CPs > 0.50 ellipse is 53.71° with
598 a bootstrapped 95% confidence interval of $[34.92^\circ \text{ } 68.60^\circ]$, indicating it is elongated along
599 quadrants I and III. The orientation of the major axis for the CPs < 0.50 ellipse is 153.67° with a
600 bootstrapped 95% confidence interval of $[142.53^\circ \text{ } 165.04^\circ]$, indicating it is elongated along
601 quadrants II and IV. Thus, in CIP, neurons with CPs > 0.50 tend to have slant and choice partial
602 correlations of the same sign, whereas neurons with CPs < 0.50 tend to have slant and choice
603 partial correlations of opposite sign. The slant and choice partial correlations in CIP were not
604 significantly correlated with each other overall ($r = -0.17$, $p = 0.18$), suggesting that slant and
605 choice can have independent effects on neuronal responses (see Discussion).

606 In V3A, the mean CP for quadrants I and III (0.55 ± 0.03 SEM) was not significantly
607 greater than 0.50 ($N = 9$, Wilcoxon signed rank test, $p = 0.09$), but the mean CP for quadrants II

608 and IV (0.44 ± 0.02 SEM) was significantly less than 0.50 ($N = 14$, Wilcoxon signed rank test, p
609 $= 0.02$). This suggests there was some tendency for the relative signs of the slant and choice
610 partial correlations to predict CP in V3A. However, this trend was weak compared to CIP, as
611 demonstrated by the 95% confidence ellipses for CPs > 0.50 and CPs < 0.50 in V3A. For both
612 ellipses, the major axis is oriented approximately along the slant partial correlation axis (1.08°
613 and -3.53° for CPs > 0.50 and CPs < 0.50 , respectively), reflecting that the V3A responses were
614 substantially more dependent on slant than choice.

615

616

617 **Time course of stimulus-related and choice-related activity in CIP and V3A**

618 Lastly, we examined the time course of CPs, neuronal thresholds, and partial
619 correlations in CIP and V3A by computing these quantities within a series of 200 ms bins shifted
620 every 50 ms. Average CP time courses are shown in Fig. 8A,B for CIP and V3A, respectively.
621 The mean CIP CP increased above baseline relatively late in the stimulus duration and
622 remained elevated. The first time bin in which the mean CP (0.53 ± 0.01 SEM, $N = 65$ neurons)
623 was significantly greater than 0.50 was 350 ms (bin center) after stimulus onset (one-way
624 ANOVA with multiple comparisons for $N = 22$ time bins, $p < 0.05$). The CP plateaued around
625 400 ms after stimulus onset and maintained this approximate level until the last time bin before
626 stimulus offset (950 ms), at which point there was a further increase in CP which may reflect
627 additional choice-related activity and/or directionally selective saccade-related activity. The
628 mean V3A CP was not significantly different from 0.50 in any time bin (one-way ANOVA with
629 multiple comparisons for $N = 22$ time bins, $p \geq 0.05$), but was slightly less than 0.50 throughout
630 most of the stimulus duration. For comparison, mean CIP and V3A neuronal thresholds are
631 shown in Fig. 8C,D, respectively.

632 The mean time courses for the spike density function (SDF; a measure of the average
633 population response), squared slant partial correlation (SPC), and squared choice partial
634 correlation (CPC) are shown for CIP and V3A in Fig. 8E,F, respectively. The time courses of the
635 squared slant partial correlations (black curves) are highly similar to the mean spike density
636 functions (blue curves), with an early peak and smaller sustained values. In fact, the time course
637 of the spike density function was highly correlated with that of the slant partial correlation in both
638 areas (CIP: $r = 0.93$, $p = 2.4 \times 10^{-10}$, $N = 22$; V3A: $r = 0.90$, $p = 1.9 \times 10^{-8}$, $N = 22$). In CIP, the time
639 course of the squared slant partial correlation peaked around 250-300 ms (bin centers),
640 whereas the squared choice partial correlation increased later during the stimulus epoch (red
641 curve). It was not until 450 ms (bin center) after stimulus onset that the squared choice partial

642 correlation became significantly different from its initial value (one-way ANOVA with multiple
643 comparisons, $p < 0.05$), further emphasizing that choice-related activity in CIP is substantially
644 delayed relative to stimulus-related activity. Similar to the CP time course, the squared choice
645 partial correlation plateaued until about the time of stimulus offset, at which point it increased
646 further. In contrast, for V3A, the squared choice partial correlation remained close to zero
647 throughout the stimulus duration, further reflecting that there was little to no choice-related
648 activity in V3A. The squared choice partial correlation for V3A did, however, increase
649 significantly above its initial value after stimulus offset, at the 1,100 and 1,150 ms time bins
650 (one-way ANOVA with multiple comparison, $p < 0.05$). Given that the V3A CP was not
651 significantly different from 0.50 in these same time bins (indicating that the increase in squared
652 choice partial correlation was not linked to choices made in the direction of the neurons'
653 preferred vs. non-preferred slant signs), and given that a previous study reported saccade-
654 related activity in V3A (Nakamura and Colby, 2000), the increase in squared choice partial
655 correlation following stimulus offset might be caused by directionally selective saccade-related
656 activity.

657

658 **DISCUSSION**

659 We investigated correlations between 3D surface orientation perception and neuronal
660 activity in areas V3A and CIP of the macaque monkey. Our results show that surface orientation
661 is similarly discriminable based on V3A and CIP responses, and that neurons in the two areas
662 are similarly sensitive to small slant variations. Together with anatomical data (Nakamura et al.,
663 2001), these results suggest V3A may, at least partially, underlie 3D orientation selectivity in
664 CIP (Taira et al., 2000; Tsutsui et al., 2001; Rosenberg et al., 2013; Rosenberg and Angelaki,
665 2014b). Although stimulus-related activity was similar in the two areas, choice-related activity
666 differed qualitatively. Specifically, choice-related activity during the slant discrimination task was
667 prominent in CIP but largely lacking in V3A, implying a functional distinction between the areas.
668 Together, these results suggest that both areas may contribute to 3D surface orientation
669 processing, but only CIP carries prominent 3D orientation choice-related signals.

670

671 **Comparison of stimulus-related and choice-related activity in CIP and V3A**

672 The present results strongly agree with previous reports of 3D orientation selectivity in
673 CIP (Taira et al., 2000; Rosenberg et al., 2013), and are consistent with previous studies
674 implicating V3A in binocular disparity processing, 3D vision, and prehensile sensorimotor
675 processing (Nakamura et al., 2001; Tsao et al., 2003; Anzai et al., 2011; Ban and Welchman,

676 2015; Goncalves et al., 2015). In both areas, 3D orientation preferences were shifted towards
677 small slant preferences. This non-uniformity differs from our previous finding of a uniform
678 distribution of 3D orientation preferences in CIP (Rosenberg et al., 2013), and may be a
679 byproduct of extensive slant discrimination training about the frontoparallel plane. Based on 3D
680 orientation tuning measured during passive fixation, the strength of selectivity was similar
681 between the two areas (quantified using the SODI), though slightly greater in V3A than CIP.
682 When slant tuning was measured during the slant discrimination task, V3A and CIP neurons
683 were similarly sensitive to small slant changes, as evidenced by similar average neuronal
684 thresholds. For some neurons in each area, neuronal thresholds were nearly as small as the
685 behavioral threshold, suggesting that the monkeys may be less sensitive to changes in slant
686 than is possible from an optimal decoding of the neuronal activity. Recent theoretical work
687 suggests that sub-optimal decoding and/or information-limiting noise correlations that introduce
688 redundancy may cause behavioral thresholds to be only slightly smaller than individual neuronal
689 thresholds (Moreno-Bote et al., 2014; Pitkow et al., 2015).

690 Although we found similar stimulus response properties in V3A and CIP, there was a
691 stark difference in their choice-related activity. More than half of the CIP neurons had significant
692 CPs, whereas only one V3A neuron had a significant CP. This difference suggests that CIP
693 activity is functionally coupled with perceptual slant decisions, whereas V3A activity is not.
694 However, given the small number of V3A neurons recorded in this study, this result should be
695 considered preliminary. Additionally, the relationship between CIP activity and choice is not
696 necessarily causal. Significant CPs could arise in a bottom-up manner (Britten et al., 1996;
697 Haefner et al., 2013; Wimmer et al., 2015), but there is growing evidence that top-down
698 (feedback) signals make important contributions to the presence of CPs (Nienborg and
699 Cumming, 2009; Wimmer et al., 2015; Cumming and Nienborg, 2016; Kwon et al., 2016; Yang
700 et al., 2016). Thus, observing significant choice-related activity does not necessarily imply a
701 contribution to perceptual decisions, as reinforced by recent findings of dissociations between
702 choice-related activity and reversible inactivation of brain areas. For example, macaque VIP
703 neurons have substantially greater CPs than MSTd neurons during a heading discrimination
704 task (Gu et al., 2007; Gu et al., 2008; Chen et al., 2013), yet inactivation of MSTd impairs task
705 performance whereas inactivation of VIP does not (Gu et al., 2012; Chen et al., 2016). Similarly,
706 macaque LIP shows robust choice-related activity during motion discrimination, but inactivation
707 of LIP does not impair task performance (Katz et al., 2016). A causal relationship between 3D
708 surface orientation perception and CIP activity thus remains uncertain.

709 Previous work has shown that the 3D orientation tuning of CIP neurons is largely
710 invariant to changes in the mean depth of the stimuli relative to the fixation plane, as well as the
711 defining visual (i.e., perspective or stereoscopic) cue, suggesting that CIP neurons are sensitive
712 to depth gradients (Taira et al., 2000; Tsutsui et al., 2001; Rosenberg and Angelaki, 2014b). In
713 the present study, we did not have sufficient stimulus conditions to determine if the slant
714 selectivity of V3A neurons is also robust to changes in mean depth. Thus, we cannot rule out
715 the possibility that the selectivity we observed in V3A reflects local disparity selectivity, given
716 that local disparity within the receptive field changes as a function of slant in our stimulus.
717 Indeed, an intriguing hypothesis is that our finding of robust CPs in CIP, but not in V3A, may be
718 related to the extent to which these areas represent slant in a manner that is tolerant to
719 variations in other cues (e.g., mean disparity). Specifically, it is possible that the lack of CPs in
720 V3A results from a lack of tolerance to changes in mean disparity. We are currently conducting
721 experiments to test this hypothesis directly.

722

723 **Dissociating the contributions of stimulus and choice to CIP and V3A activity**

724 To dissociate the contributions of stimulus slant and choice to CIP and V3A responses,
725 we computed partial correlations between these variables and the spike counts of individual
726 neurons. In both areas, we found strong correlations between the stimulus and spike count. In
727 contrast, correlations between choice and spike count were generally strong in CIP, but weak in
728 V3A. This analysis validates the main CP finding; namely, there was strong choice-related
729 activity in CIP but not V3A. These results are reminiscent of a previous study which found that
730 V2, but not V1, neurons show significant choice-related activity during a disparity discrimination
731 task (Nienborg and Cumming, 2006), despite the areas having similar disparity sensitivity. Thus,
732 one potential explanation for these findings is that CPs observed in V2/CIP arise primarily from
733 top-down signals that do not propagate back as strongly to V1/V3A. Another possibility, which is
734 not mutually exclusive, is that the structure of correlated noise is different between V2/CIP and
735 V1/V3A, reflecting that the appearance of CPs may depend on correlated noise (Shadlen et al.,
736 1996; Nienborg and Cumming, 2006; Haefner et al., 2013) and perhaps particularly depend on
737 correlated noise that is information-limiting for the task at hand (Pitkow et al., 2015). An
738 additional possibility, as noted above, is that CIP contains a more invariant representation of
739 slant than V3A.

740 The pattern of slant and choice partial correlations observed in CIP may reflect a
741 substantial top-down contribution to CPs. In a feedforward (bottom-up) scheme, it would be
742 expected that stimulus and choice partial correlations would have the same sign, such that

743 greater activity from a neuron constitutes evidence in favor of its preferred stimulus. In contrast,
744 our CIP data show no significant relationship between slant and choice partial correlations (Fig.
745 7A). In other words, slant and choice signals are dissociated in CIP, similar to heading and
746 choice signals in VIP (Zaidel et al., 2017). This dissociation may result from top-down choice-
747 related signals that do not target CIP neurons according to their stimulus preferences.

748 It is also possible that some of the choice-related activity that we observed in CIP was
749 due to directionally selective saccade-related activity. However, the time courses of CP and
750 squared choice partial correlation suggest that any saccade-related activity may be limited to
751 the time period between stimulus offset and saccade execution. First, choice-related activity
752 became significant about 400 ms after stimulus onset (more than 800 ms before the median
753 choice time). The choice-related activity then plateaued at an elevated value until about the time
754 of stimulus offset. Second, there was a sharp increase in choice-related activity starting around
755 stimulus offset, which may reflect a choice signal and/or directionally selective saccade-related
756 activity. Together, these observations suggest that by restricting our analyses of choice activity
757 to the stimulus presentation period, we largely isolated choice-related (rather than saccade-
758 related) signals.

759 We lastly consider the relative timing of slant and choice signals. The time courses of
760 slant-related signals in CIP and V3A were highly correlated with population-level spike density
761 functions (Fig. 8). In CIP, the time courses of slant-related and choice-related signals differed
762 substantially. Whereas the time course of the slant-related signals peaked around 250-300 ms
763 after stimulus onset, the choice-related signals did not become significant until around 400 ms
764 after stimulus onset. Late-onset choice-related activity has also been observed in other dorsal
765 stream areas including MT (Dodd et al., 2001) and AIP (Verhoef et al., 2010), and may be
766 consistent with a top-down origin of choice signals in CIP, as suggested above based on the
767 lack of correlation between slant and choice signals. Also consistent with this possibility, a
768 previous study found reaction times on the order of 250-350 ms in a convex-concave
769 discrimination task (Verhoef et al., 2012), which is earlier than the start of significant choice-
770 related activity that we found in CIP. Together, the present findings implicate V3A and CIP in 3D
771 orientation processing, and suggest a qualitative distinction between the areas since only CIP
772 showed choice-related activity during a fine slant discrimination task.

773

774 REFERENCES

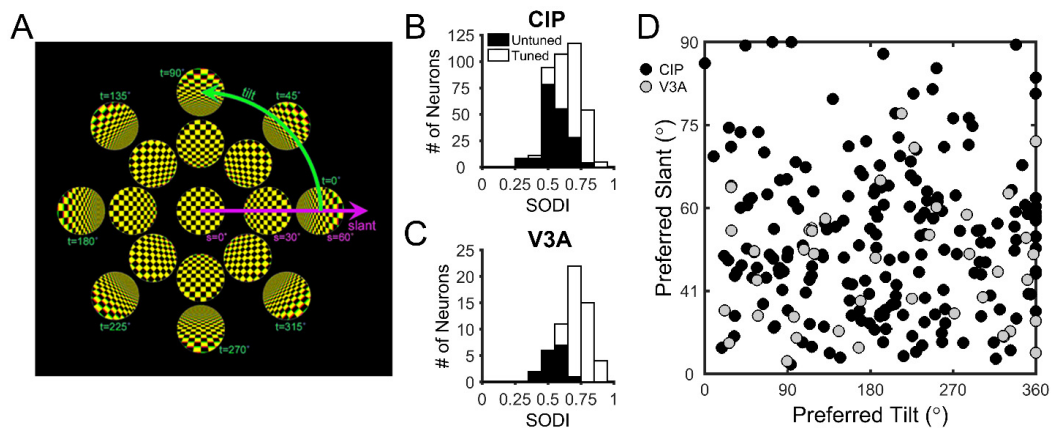
775 Alizadeh AM, Van Dromme I, Verhoef BE, Janssen P (2018) Caudal Intraparietal Sulcus and
776 three-dimensional vision: A combined functional magnetic resonance imaging and
777 single-cell study. *Neuroimage* 166:46-59.

- 778 Anzai A, Chowdhury SA, DeAngelis GC (2011) Coding of stereoscopic depth information in
779 visual areas V3 and V3A. *J Neurosci* 31:10270-10282.
- 780 Ban H, Welchman AE (2015) fMRI Analysis-by-Synthesis Reveals a Dorsal Hierarchy That
781 Extracts Surface Slant. *J Neurosci* 35:9823-9835.
- 782 Britten KH, Newsome WT, Shadlen MN, Celebrini S, Movshon JA (1996) A relationship between
783 behavioral choice and the visual responses of neurons in macaque MT. *Vis Neurosci*
784 13:87-100.
- 785 Celebrini S, Newsome WT (1994) Neuronal and psychophysical sensitivity to motion signals in
786 extrastriate area MST of the macaque monkey. *J Neurosci* 14:4109-4124.
- 787 Chen A, Deangelis GC, Angelaki DE (2013) Functional specializations of the ventral
788 intraparietal area for multisensory heading discrimination. *J Neurosci* 33:3567-3581.
- 789 Chen A, Gu Y, Liu S, DeAngelis GC, Angelaki DE (2016) Evidence for a Causal Contribution of
790 Macaque Vestibular, But Not Intraparietal, Cortex to Heading Perception. *J Neurosci*
791 36:3789-3798.
- 792 Cumming BG, Nienborg H (2016) Feedforward and feedback sources of choice probability in
793 neural population responses. *Curr Opin Neurobiol* 37:126-132.
- 794 Dodd JV, Eke K, Cumming BG, Parker AJ (2001) Perceptually bistable three-dimensional
795 figures evoke high choice probabilities in cortical area MT. *J Neurosci* 21:4809-4821.
- 796 Durand JB, Nelissen K, Joly O, Wardak C, Todd JT, Norman JF, Janssen P, Vanduffel W,
797 Orban GA (2007) Anterior regions of monkey parietal cortex process visual 3D shape.
798 *Neuron* 55:493-505.
- 799 Galletti C, Battaglini PP (1989) Gaze-dependent visual neurons in area V3A of monkey
800 prestriate cortex. *J Neurosci* 9:1112-1125.
- 801 Goncalves NR, Ban H, Sanchez-Panchuelo RM, Francis ST, Schluppeck D, Welchman AE
802 (2015) 7 tesla fMRI reveals systematic functional organization for binocular disparity in
803 dorsal visual cortex. *J Neurosci* 35:3056-3072.
- 804 Gu Y, DeAngelis GC, Angelaki DE (2007) A functional link between area MSTd and heading
805 perception based on vestibular signals. *Nat Neurosci* 10:1038-1047.
- 806 Gu Y, Angelaki DE, Deangelis GC (2008) Neural correlates of multisensory cue integration in
807 macaque MSTd. *Nat Neurosci* 11:1201-1210.
- 808 Gu Y, Deangelis GC, Angelaki DE (2012) Causal links between dorsal medial superior temporal
809 area neurons and multisensory heading perception. *J Neurosci* 32:2299-2313.
- 810 Haefner RM, Gerwinn S, Macke JH, Bethge M (2013) Inferring decoding strategies from choice
811 probabilities in the presence of correlated variability. *Nat Neurosci* 16:235-242.
- 812 Hillis JM, Watt SJ, Landy MS, Banks MS (2004) Slant from texture and disparity cues: optimal
813 cue combination. *J Vis* 4:967-992.
- 814 Hinkle DA, Connor CE (2002) Three-dimensional orientation tuning in macaque area V4. *Nat*
815 *Neurosci* 5:665-670.
- 816 Kang I, Maunsell JH (2012) Potential confounds in estimating trial-to-trial correlations between
817 neuronal response and behavior using choice probabilities. *J Neurophysiol* 108:3403-
818 3415.
- 819 Katz LN, Yates JL, Pillow JW, Huk AC (2016) Dissociated functional significance of decision-
820 related activity in the primate dorsal stream. *Nature* 535:285-288.
- 821 Kwon SE, Yang H, Minamisawa G, O'Connor DH (2016) Sensory and decision-related activity
822 propagate in a cortical feedback loop during touch perception. *Nat Neurosci* 19:1243-
823 1249.
- 824 Lewis JW, Van Essen DC (2000) Mapping of architectonic subdivisions in the macaque
825 monkey, with emphasis on parieto-occipital cortex. *J Comp Neurol* 428:79-111.
- 826 Liu Y, Vogels R, Orban GA (2004) Convergence of depth from texture and depth from disparity
827 in macaque inferior temporal cortex. *J Neurosci* 24:3795-3800.

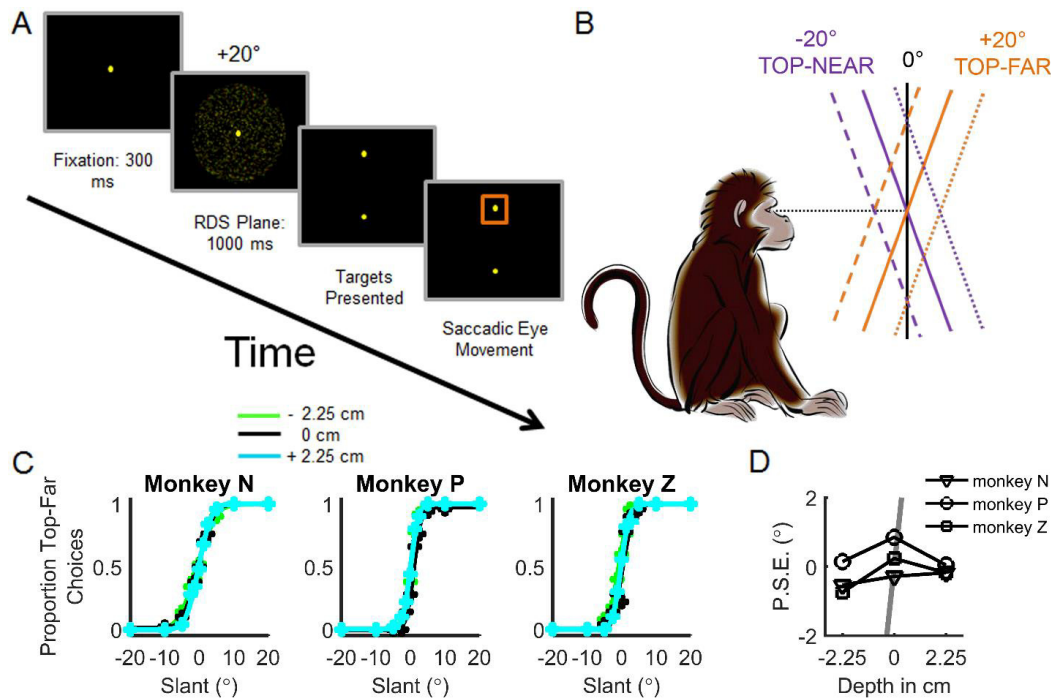
- 828 Moreno-Bote R, Beck J, Kanitscheider I, Pitkow X, Latham P, Pouget A (2014) Information-
829 limiting correlations. *Nat Neurosci* 17:1410-1417.
- 830 Murata A, Gallese V, Luppino G, Kaseda M, Sakata H (2000) Selectivity for the shape, size, and
831 orientation of objects for grasping in neurons of monkey parietal area AIP. *J*
832 *Neurophysiol* 83:2580-2601.
- 833 Nakamura H, Kuroda T, Wakita M, Kusunoki M, Kato A, Mikami A, Sakata H, Itoh K (2001)
834 From three-dimensional space vision to prehensile hand movements: The lateral
835 intraparietal area links the area V3A and the anterior intraparietal area in macaques. *J*
836 *Neurosci* 21:8174-8187.
- 837 Nakamura K, Colby CL (2000) Visual, saccade-related, and cognitive activation of single
838 neurons in monkey extrastriate area V3A. *J Neurophysiol* 84:677-692.
- 839 Nguyenkim JD, DeAngelis GC (2003) Disparity-based coding of three-dimensional surface
840 orientation by macaque middle temporal neurons. *J Neurosci* 23:7117-7128.
- 841 Nienborg H, Cumming BG (2006) Macaque V2 neurons, but not V1 neurons, show choice-
842 related activity. *J Neurosci* 26:9567-9578.
- 843 Nienborg H, Cumming BG (2009) Decision-related activity in sensory neurons reflects more
844 than a neuron's causal effect. *Nature* 459:89-92.
- 845 Pitkow X, Liu S, Angelaki DE, DeAngelis GC, Pouget A (2015) How can single sensory neurons
846 predict behavior? *Neuron* 87:411-423.
- 847 Prince SJ, Pointon AD, Cumming BG, Parker AJ (2002) Quantitative analysis of the responses
848 of V1 neurons to horizontal disparity in dynamic random-dot stereograms. *J*
849 *Neurophysiol* 87:191-208.
- 850 Rosenberg A, Angelaki DE (2014a) Gravity influences the visual representation of object tilt in
851 parietal cortex. *J Neurosci* 34:14170-14180.
- 852 Rosenberg A, Angelaki DE (2014b) Reliability-dependent contributions of visual orientation cues
853 in parietal cortex. *Proc Natl Acad Sci U S A* 111:18043-18048.
- 854 Rosenberg A, Cowan NJ, Angelaki DE (2013) The visual representation of 3D object orientation
855 in parietal cortex. *J Neurosci* 33:19352-19361.
- 856 Sanada TM, Nguyenkim JD, Deangelis GC (2012) Representation of 3-D surface orientation by
857 velocity and disparity gradient cues in area MT. *J Neurophysiol* 107:2109-2122.
- 858 Shadlen MN, Britten KH, Newsome WT, Movshon JA (1996) A computational analysis of the
859 relationship between neuronal and behavioral responses to visual motion. *J Neurosci*
860 16:1486-1510.
- 861 Sugihara H, Murakami I, Shenoy KV, Andersen RA, Komatsu H (2002) Response of MSTd
862 neurons to simulated 3D orientation of rotating planes. *J Neurophysiol* 87:273-285.
- 863 Taira M, Tsutsui KI, Jiang M, Yara K, Sakata H (2000) Parietal neurons represent surface
864 orientation from the gradient of binocular disparity. *J Neurophysiol* 83:3140-3146.
- 865 Tsao DY, Vanduffel W, Sasaki Y, Fize D, Knutsen TA, Mandeville JB, Wald LL, Dale AM, Rosen
866 BR, Van Essen DC, Livingstone MS, Orban GA, Tootell RB (2003) Stereopsis activates
867 V3A and caudal intraparietal areas in macaques and humans. *Neuron* 39:555-568.
- 868 Tsutsui K, Jiang M, Yara K, Sakata H, Taira M (2001) Integration of perspective and disparity
869 cues in surface-orientation-selective neurons of area CIP. *J Neurophysiol* 86:2856-2867.
- 870 Tummers B (2006) DataThief III. In: <http://datathief.org/>.
- 871 Van Dromme IC, Premereur E, Verhoef B-E, Vanduffel W, Janssen P (2016) Posterior Parietal
872 Cortex Drives Inferotemporal Activations During Three-Dimensional Object Vision. *PLOS*
873 *Biol* 14:e1002445.
- 874 Van Essen DC, Lewis JW, Drury HA, Hadjikhani N, Tootell RB, Bakircioglu M, Miller MI (2001)
875 Mapping visual cortex in monkeys and humans using surface-based atlases. *Vision Res*
876 41:1359-1378.
- 877 Verhoef BE, Vogels R, Janssen P (2010) Contribution of inferior temporal and posterior parietal
878 activity to three-dimensional shape perception. *Curr Biol* 20:909-913.

- 879 Verhoef BE, Vogels R, Janssen P (2012) Inferotemporal cortex subserves three-dimensional
880 structure categorization. *Neuron* 73:171-182.
- 881 Wichmann FA, Hill NJ (2001) The psychometric function: I. Fitting, sampling, and goodness of
882 fit. *Percept Psychophys* 63:1293-1313.
- 883 Wimmer K, Compte A, Roxin A, Peixoto D, Renart A, de la Rocha J (2015) Sensory integration
884 dynamics in a hierarchical network explains choice probabilities in cortical area MT. *Nat*
885 *Commun* 6:6177.
- 886 Yang H, Kwon SE, Severson KS, O'Connor DH (2016) Origins of choice-related activity in
887 mouse somatosensory cortex. *Nat Neurosci* 19:127-134.
- 888 Zaidel A, DeAngelis GC, Angelaki DE (2017) Decoupled choice-driven and stimulus-related
889 activity in parietal neurons may be misrepresented by choice probabilities. *Nat Commun*
890 8:715.
- 891 Zeki SM (1978a) Uniformity and diversity of structure and function in rhesus monkey prestriate
892 visual cortex. *J Physiol* 277:273-290.
- 893 Zeki SM (1978b) The third visual complex of rhesus monkey prestriate cortex. *J Physiol*
894 277:245-272.
- 895 Zeki SM (1978c) Functional specialisation in the visual cortex of the rhesus monkey. *Nature*
896 274:423-428.

897 FIGURES AND FIGURE LEGENDS

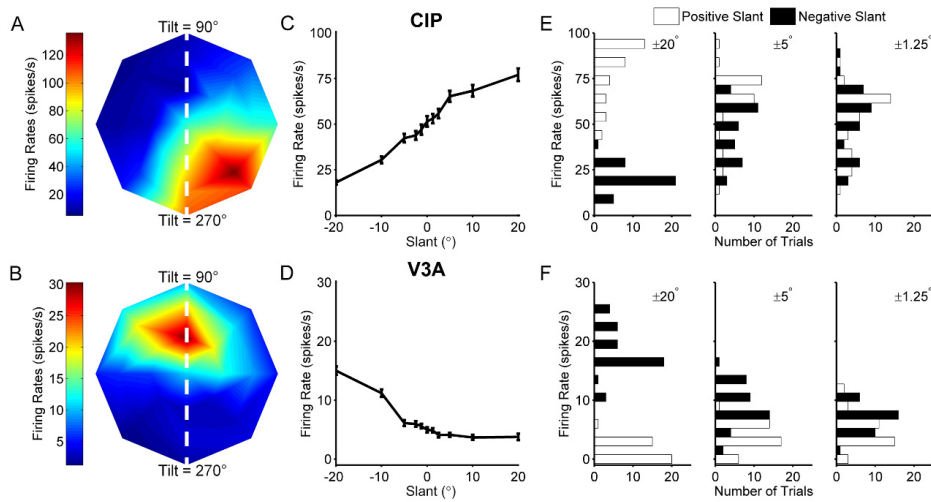


898
 899 **Figure 1.** Surface orientation tuning. **A**, The 3D orientation of a planar surface can be described
 900 by two variables, slant and tilt. Tilt specifies the axis within the frontoparallel plane about which
 901 the plane is rotated, and slant specifies how much it is rotated. These variables define a polar
 902 coordinate system. Only a subset of the stimuli used in the study are shown. **B & C**,
 903 Distributions of the surface orientation discrimination index (SODI) for 396 CIP (**B**) and 60 V3A
 904 (**C**) neurons. Open bars denote tuned neurons (215 CIP and 44 V3A), and filled bars denote
 905 untuned neurons (181 CIP and 16 V3A). **D**, Equal area projection (Rosenberg et al., 2013)
 906 showing joint distribution of preferred slants and tilts for the 215 tuned CIP neurons (black circles)
 907 and 44 tuned V3A neurons (gray circles).



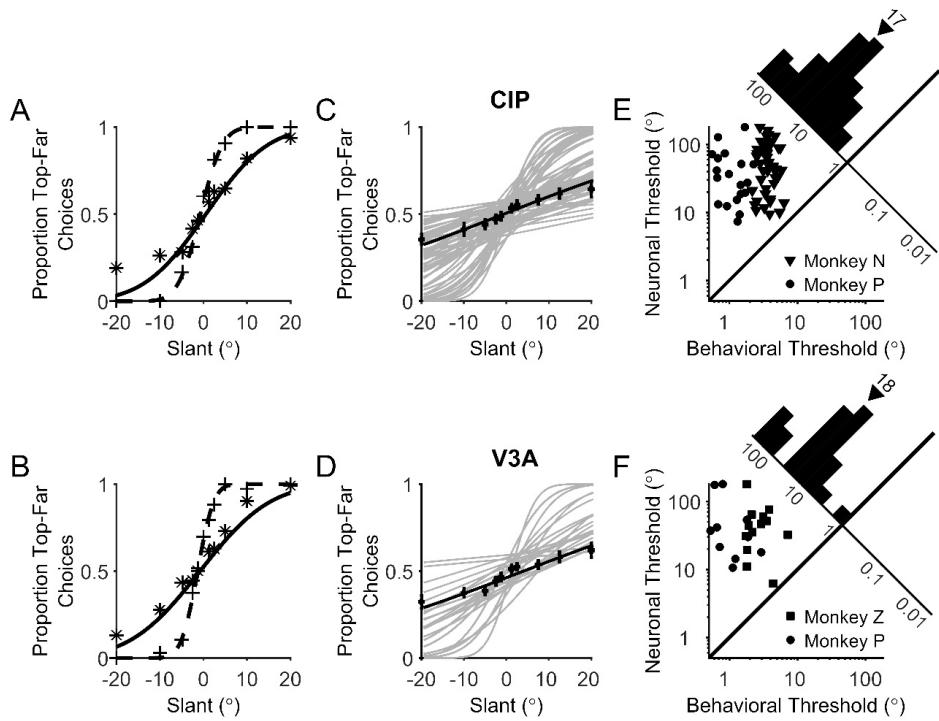
908

909 **Figure 2.** Slant discrimination task and behavioral performance. **A**, Temporal sequence of
 910 events in the slant discrimination task. Each trial began with the presentation of a fixation point
 911 at the center of the screen. The monkey fixated this point for 300 ms after which a random dot
 912 stereogram (RDS) plane was presented for 1,000 ms while fixation was maintained. The
 913 monkey then reported which direction the plane was slanted away from frontoparallel by making
 914 a saccade to the upper target if the slant was positive (top-far) or the lower target if the slant
 915 was negative (top-near). **B**, Side view of the task illustrating positive versus negative slants.
 916 Solid lines depict planes centered at the fixation depth (screen distance ~ 32.5 cm). Dashed and
 917 dotted lines depict planes centered at either near or far depths (2.25 cm in front of or behind the
 918 display), respectively. **C**, Discrimination behavior plotted as the proportion of top-far choices as
 919 a function of slant. Data are fit with a cumulative Gaussian for each depth ($N = 450$ trials/data
 920 point). **D**, The point of subjective equality (P.S.E.) as a function of depth for each monkey. For
 921 comparison, the gray line shows the expected dependency of the P.S.E. on stimulus depth if the
 922 task was performed based on local absolute disparities rather than slant. The line reaches $\pm 14^\circ$
 923 at ± 2.25 cm but is clipped at $\pm 2^\circ$ to not obscure the data.



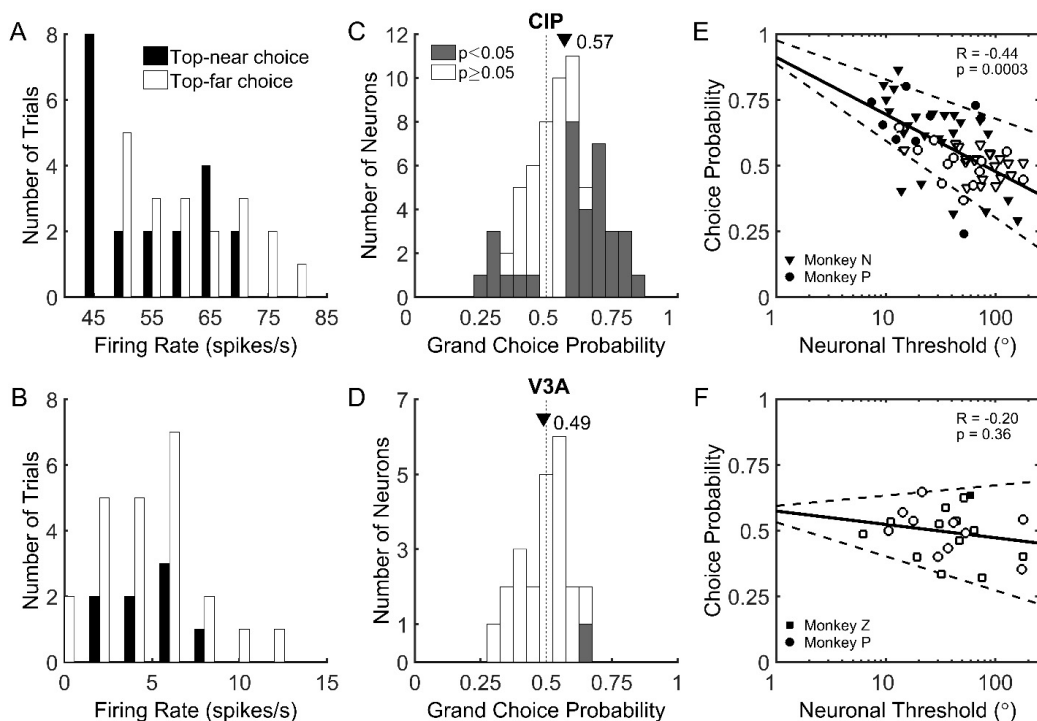
924

925 **Figure 3.** Surface orientation tuning of example CIP and V3A neurons. **A & B**, Slant-tilt tuning
 926 profiles of representative CIP (**A**) and V3A (**B**) neurons. Firing rate is color coded with red hues
 927 indicating larger firing rates. The peak of the CIP tuning profile is in the lower right corner,
 928 indicating that the cell responded best to a planar surface with the lower right corner closest to
 929 the monkey. The peak of the V3A tuning profile is in the upper portion of the plot, indicating that
 930 the cell responded best to a planar surface with the top closest to the monkey. White dashed
 931 lines correspond to the 90°/270° tilt axis along which the slant discrimination task was
 932 performed. **C & D**, Slant tuning curves of the same CIP (**C**) and V3A (**D**) neurons measured
 933 during the slant discrimination task. Error bars denote SEM. **E & F**, Neuronal response
 934 distributions for three pairs of slant angles ($\pm 20^\circ$, $\pm 5^\circ$, $\pm 1.25^\circ$) for the CIP (**E**) and V3A (**F**)
 935 neurons. Negative slants are shown as black bars and positive slants are shown as white bars.



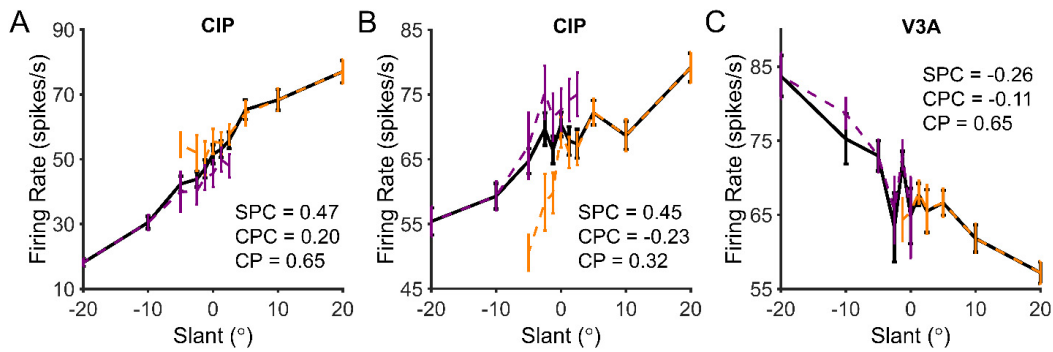
936

937 **Figure 4.** Comparison of behavioral and neuronal sensitivity. **A & B**, The proportion of 'top-far'
 938 choices made during the recordings of the CIP (**A**) and V3A (**B**) neurons from Fig. 3 are plotted
 939 as a function of slant ('+'s). Simultaneously measured neuronal responses were converted into
 940 neurometric functions using ROC analysis and the proportion of 'top-far' choices of an ideal
 941 observer are plotted as a function of slant ('*'s). Dashed and solid curves show cumulative
 942 Gaussian fits to the psychometric and neurometric functions, respectively. **C & D**, Gray curves
 943 show cumulative Gaussian fits to the neurometric functions of each neuron recorded during the
 944 slant discrimination task. Black symbols and curves show average neurometric functions across
 945 animals and neurons. Error bars denote SEM. **E & F**, Behavioral and neuronal thresholds are
 946 compared for all individual experiments for monkeys N (triangles), P (circles), and Z (squares)
 947 for CIP (**E**) and V3A (**F**). Neuronal thresholds are multiplied by $\sqrt{2}$ to account for the
 948 neuron/anti-neuron comparison. Diagonal histograms show distributions of neuronal to
 949 behavioral threshold ratios. Triangles above the histograms mark median threshold ratios.



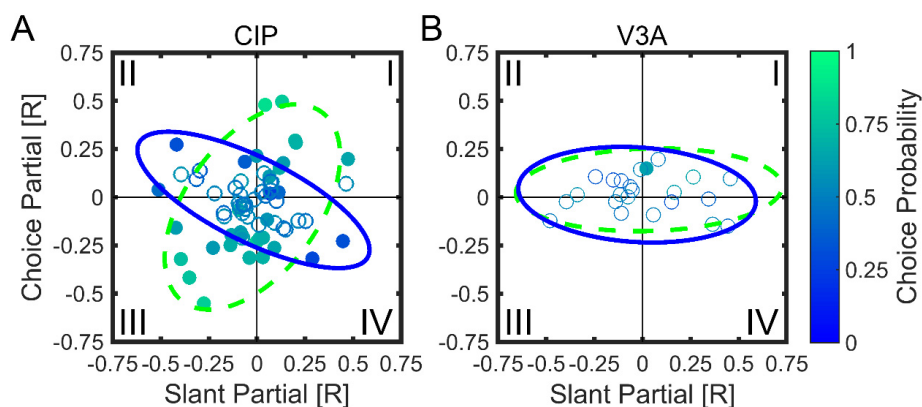
950

951 **Figure 5.** Summary of choice-related activity in CIP and V3A. **A & B**, Distribution of firing rates
 952 for example CIP (**A**) and V3A (**B**) neurons (same as in Figs. 3, 4A,B) in response to the
 953 ambiguous 0° slant stimulus. Responses are sorted according to whether the monkey made a
 954 ‘top-near’ (black) or ‘top-far’ (white) choice. For the CIP neuron, the choice-related difference in
 955 responses yielded a choice probability significantly different from chance (grand CP = 0.65, $p =$
 956 0.001). For the V3A neuron, there was no significant choice-related difference in responses
 957 (grand CP = 0.50, $p = 0.36$). **C & D**, Histograms of grand choice probabilities for all 65 CIP (**C**)
 958 and 23 V3A (**D**) neurons. Gray bars denote CPs that are significantly different from the chance
 959 value of 0.50 ($p < 0.05$, permutation test). Mean CPs are marked by triangles. **E & F**, Choice
 960 probability as a function of neuronal threshold (multiplied by $\sqrt{2}$). There is a significant negative
 961 correlation between CP and neuronal threshold in CIP (**E**) and no significant correlation
 962 between CP and neuronal threshold in V3A (**F**). Solid lines show linear fits and dashed lines
 963 show 95% confidence intervals for the slope. Filled symbols denote CPs significantly different
 964 from chance (0.50, $p < 0.05$, permutation test). Different symbols correspond to different
 965 animals.



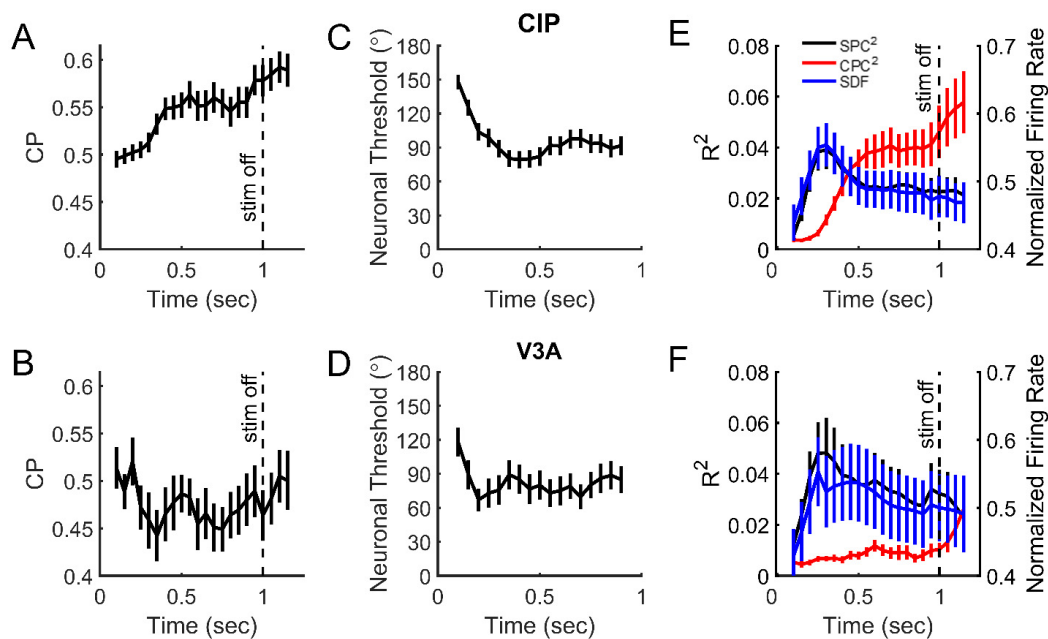
966

967 **Figure 6.** Example CIP and V3A neurons illustrating the effect of choice on slant tuning. For
 968 each neuron, the black curve shows the slant tuning curve created by averaging responses
 969 regardless of choice. Orange and purple curves show choice-conditioned slant tuning curves
 970 created by separating responses into top-far versus top-near choices, respectively. The slant
 971 partial correlation (SPC), choice partial correlation (CPC), and choice probability (CP) are listed
 972 for each neuron. **A**, CIP neuron with a positive SPC, a positive CPC, and a CP > 0.50 ($p =$
 973 0.001). **B**, CIP neuron with a positive SPC, a negative CPC, and a CP < 0.50 ($p =$
 974 0.001). **C**, V3A neuron with a negative SPC, a negative CPC, and a CP > 0.50 ($p =$ 0.29).



975

976 **Figure 7.** Partial correlation analysis showing relationships between slant partial correlation,
 977 choice partial correlation, and CP. Choice partial correlation is plotted as a function of slant
 978 partial correlation with individual neurons color coded to indicate CP. Significant CPs are filled,
 979 nonsignificant CPs are open. Data are shown for 65 CIP (**A**) and 23 V3A (**B**) neurons. Curves
 980 show 95% confidence ellipses fit to data points with CP > 0.50 (green dashed) or CP < 0.50
 981 (blue solid). **A**, In CIP, as indicated by the oblique orientations of the 95% confidence ellipses,
 982 CPs > 0.50 (greener) tended to occur when the slant and choice partial correlations had the
 983 same sign (quadrants I and III) whereas CPs < 0.50 (bluer) tended to occur when the slant and
 984 choice partial correlations had opposite signs (quadrants II and IV). **B**, For V3A, choice-related
 985 activity was weak, as indicated by the elongated but horizontally oriented 95% confidence
 986 ellipses.



987

988 **Figure 8.** Time courses of choice probability, neuronal threshold, and partial correlations. **A &**
 989 **B,** Mean values of choice probability (CP) for CIP (**A**) and V3A (**B**) neurons as a function of time
 990 relative to stimulus onset. **C & D,** Mean neuronal thresholds (multiplied by $\sqrt{2}$) for CIP (**C**) and
 991 V3A (**D**) as a function of time. **E & F,** Mean spike density functions (SDF, blue) as well as
 992 squared slant (SPC, black) and choice (CPC, red) partial correlations for CIP (**E**) and V3A (**F**) as
 993 a function of time. In all plots, analysis bins are 200 ms in duration, shifted every 50 ms starting
 994 at 100 ms. Each point is plotted in the center of the 200 ms time bin. Error bars denote SEM.
 995 Vertical dashed lines in **A, B, E,** and **F** mark the end of the stimulus presentation. The last time
 996 bin is centered at 1,150 ms, and thus extends approximately until the median choice time (1,271
 997 ms after stimulus onset).